Final Report

Department of Energy
Climate and Environmental Sciences Division
Grant #DE-SC0001467

Project Title:
Transforming the representation of the boundary layer and low clouds for high-resolution regional climate modeling

PI: Alex Hall
Joint Institute for Regional Earth System Science and Engineering
University of California, Los Angeles
Los Angeles, CA 90095

1. Summary

Stratocumulus and shallow cumulus clouds in subtropical oceanic regions (e.g., Southeast Pacific) cover thousands of square kilometers and play a key role in regulating global climate (e.g., Klein and Hartmann, 1993). Numerical modeling is an essential tool to study these clouds in regional and global systems, but the current generation of climate and weather models has difficulties in representing them in a realistic way (e.g., Siebesma et al., 2004; Stevens et al., 2007; Teixeira et al., 2011).

While numerical models resolve the large-scale flow, subgrid-scale parameterizations are needed to estimate small-scale properties (e.g. boundary layer turbulence and convection, clouds, radiation), which have significant influence on the resolved scale due to the complex nonlinear nature of the atmosphere. To represent the contribution of these fine-scale processes to the resolved scale, climate models use various parameterizations, which are the main pieces in the model that contribute to the low clouds dynamics and therefore are the major sources of errors or approximations in their representation.

In this project, we aim to 1) improve our understanding of the physical processes in thermal circulation and cloud formation, 2) examine the performance and sensitivity of various parameterizations in the regional weather model (Weather Research and Forecasting model; WRF), and 3) develop, implement, and evaluate the advanced boundary layer parameterization in the regional model to better represent stratocumulus, shallow cumulus, and their transition. Thus, this project includes three major corresponding studies.

We find that the mean diurnal cycle is sensitive to model domain in ways that reveal the existence of different contributions originating from the Southeast Pacific land-masses. The experiments suggest that diurnal variations in circulations and thermal structures over this region are influenced by convection over the Peruvian sector of the Andes cordillera, while the mostly dry mountain-breeze circulations force an additional component that results in semi-diurnal variations near the coast. A series of numerical tests, however, reveal sensitivity of the simulations to the choice of vertical grid, limiting the possibility of solid quantitative statements on the amplitudes and phases of the diurnal and semidiurnal components across the domain.

According to our experiments, the Mellor-Yamada-Nakanishi-Niino (MYNN) boundary layer scheme and the WSM6 microphysics scheme is the combination of schemes that performs best. For that combination, mean cloud cover, liquid water path, and cloud depth are fairly well-simulated, while mean cloud top height remains too low in comparison to observations. Both microphysics and boundary layer schemes contribute to the spread in liquid water path and cloud depth, although the microphysics contribution is slightly more prominent. Boundary layer schemes are the primary contributors to cloud top height, degree of adiabaticity, and cloud cover. Cloud top height is closely related to surface fluxes and boundary layer structure. Thus, our study infers that an appropriate tuning of cloud top height would likely improve the low-cloud representation in the model. Finally, we show that entrainment governs the degree of adiabaticity, while boundary layer decoupling is a control on cloud cover.

In the intercomparison study using WRF single-column model experiments, most parameterizations show a poor agreement of the vertical boundary layer structure when compared with large-eddy simulation models. We also implement a new Total-Energy/Mass-Flux boundary layer scheme into the WRF model and evaluate its ability to simulate both stratocumulus and shallow cumulus clouds. Result comparisons against large-eddy simulation show that this advanced parameterization based on the new Eddy-Diffusivity/Mass-Flux approach provides a better performance than other boundary layer parameterizations.

2. Project Studies

To investigate the performance of the regional climate model on stratocumulus and shallow cumulus clouds over Southern Pacific and Atlantic Oceans, three key studies are included in this project:

I) Several numerical experiments using the WRF model are set up to examine the influence of the South American land mass and its mountains on the diurnal anomalies of the atmospheric boundary layer circulation.

II) A series of WRF simulations is performed to systematically evaluate the sensitivity and the performance of different microphysics models, planetary boundary layer parameterizations, and cumulus schemes on a stratocumulus-to-shallow-cumulus region.

III) A recently developed planetary boundary layer scheme is implemented into the WRF model. An intercomparison study using the single-column model is performed, and the results suggest this advanced scheme, unifying turbulence and moist convection components, produces a better result for both stratocumulus and shallow cumulus regimes.

2.1 Study I: Numerical modeling of diurnal cycle in the lower troposphere over the Southeast Pacific

In order to better understand the special combination of diurnal and semidiurnal features in the thermal circulation and clouds over stratocumulus regions, we first discuss the contributions to such features by several processes using the WRF numerical experiments in this study.

Figure 1 shows the model domain, which includes much of the South American land mass. The domains are smaller in the three additional sensitivity simulations, with changes in the position of the eastern boundary such as to exclude part or all of the Andes. Each simulation is initialized from midnight UTC, October 14, 2006, and the last fifteen days of October are evaluated in this study.

For the parameterizations affecting cloud formation, we selected the Kain and Fritsch cumulus scheme (Kain and Fritsch, 1993), Purdue Lin microphysics scheme (Lin et al., 1983), and Yonsei University (YSU) PBL scheme (Hong et al., 2006). The lateral boundary and initial conditions for the simulations are derived from the National Centers for Environmental Prediction's (NCEP) final analysis (FNL) fields at 1° × 1° resolution with a 6-hour interval. The boundary conditions are prescribed over a domain with the depth of 5 grid cells where prognostic variables are relaxed toward the FNL solution. The sea-surface temperatures are prescribed at the lower boundary from the daily-varying optimum interpolation reanalysis data (Reynolds and Smith, 1994).

The model grid has a central horizontal spacing of 45 km and 43 sigma levels in the vertical. In an attempt to better represent the sharp inversion at the top of the marine PBL, the vertical resolution is enhanced with 27 layers below about 800 hPa. The remaining 16 layers above this level are spaced nearly uniformly, with a vertical resolution between 50 hPa and 60 hPa in the mid-troposphere.

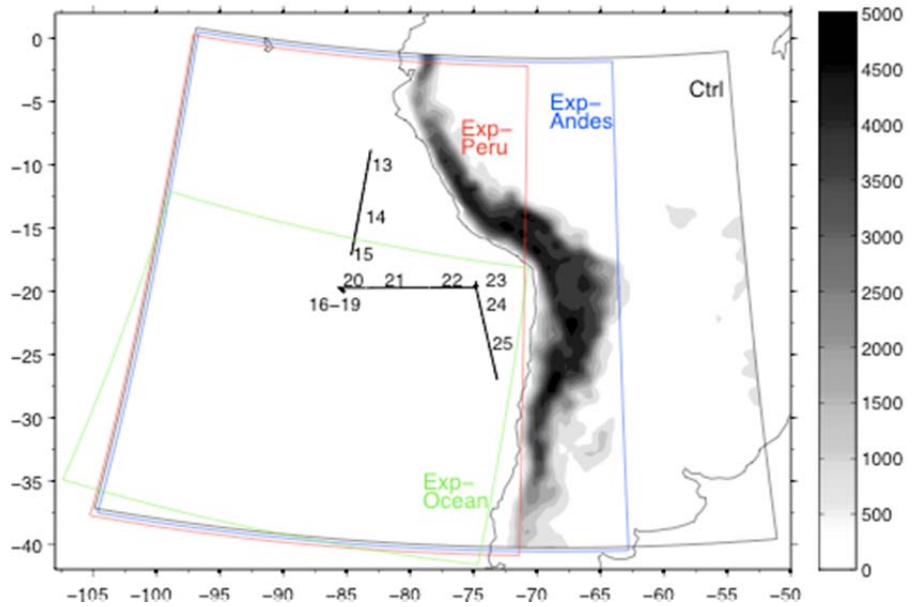

Figure 1: Map of topographic elevations (shaded, in meters) for the study area. Superimposed are transects of ship-based balloon soundings with the corresponding observing locations and dates of October 2006, and the simulation domain for the WRF control integration (black box) and for the sensitivity experiments (colored boxes).

Though these experiments, we are able to evaluate the WRF model's performance on stratocumulus and shallow cumulus region. Model results are compared to a series of observational and reanalysis datasets. The 2006 NOAA Stratus research cruise with the RV Ronald H. Brown, which took place between October 13–25 in the stratocumulus region off-shore of Chile and Peru, provided continuous ship-based measurements of surface meteorology, turbulent and radiative fluxes, cloud thickness, and optical properties. Rawinsondes were launched from the ship every 4 or 6 hours beginning October 18, providing vertical profiles of air temperature, humidity, and winds. We also use QuickSCAT scatterometer daily-mean surface wind data on a 0.5° × 0.5° grid. Finally, we use reanalysis data from the ERA-Interim project (Dee et al., 2011).

2.2 Study II: Sensitivity experiment to parameterizations in the WRF model for stratocumulus simulations in the Southeast Pacific

In this work, we examine the performance and the sensitivity of stratocumulus simulations to various parameterizations in the WRF model. Five PBL—YSU (Hong et al., 2006), ACM2 (Pleim, 2007), MYJ (Janjic, 2002), MYNN (Nakanishi and Niino, 2004), and QNSE (Sukoriansky et al., 2005)—and three MP—Lin (Lin et al., 1983), WSM6 (Hong and Lim, 2006), and Thomson (Thomson et al., 2004)—parameterizations are cross-tested (i.e., 15 simulations) during October and November 2008 for a fixed cumulus scheme without shallow CU parameterization. All PBL parameterizations and MP schemes are listed in Table 1. Average simulated low-cloud amount and structure is compared to both *in-situ* and remote sensing measurements. The study domain is the same as shown in the previous study (i.e., Figure 1).

Remotely sensed data are used to compare the performance of model parameterizations in 3D simulations. We use data from the National Aeronautics and Space Administration Moderate-resolution Imaging Spectrometer (MODIS) instrument (Platnick et al., 2003; Platnick and King,

2007). MODIS is deployed on two different sun-synchronous polar orbiting satellites, Terra and Aqua, which pass over the equator twice a day, at 10:30 AM/PM (Terra) and 1:30 AM/PM (Aqua) local time. MODIS scans are 2330 km wide. This enables MODIS to cover 90% of our region of interest four times per day, on average. The large spatial coverage makes MODIS very useful for regional climate model validation. We use two variables from MODIS for comparison to WRF. The first is cloud cover. MODIS uses a combination of several spectral bands in the near infrared to determine a cloud mask on a 1–5 km grid. The second variable used in this work is liquid water path, the integrated amount of cloud liquid water in the atmosphere column, typically expressed in g/m^2. Liquid water path is not directly measured in MODIS, but instead can be derived from retrievals of the effective radius and optical depth at the cloud top.

Comparison of model results against these valuable observations will give us not only the performance of each scheme, but also the best combination of parameterizations to select for the simulation of stratocumulus regions.

Table 1: List of boundary layer parameterizations and microphysics schemes used for the experiments in Study II.

Boundary layer parameterization

Name of parameterization	*Nomenclature*	*Selected reference*
Yonsei University	YSU	Hong et al. (2006)
Asymmetric Convective Model Ver. 2	ACM2	Pleim (2007)
Mellor-Yamada-Janjic	MYJ	Mellor and Yamada (1982); Janjic (2002)
Mellor-Yamada-Nakanishi-Niino	MYNN	Nakanishi and Niino (2004)
Quasi-Normal Scale Elimination	QNSE	Sukoriansky et al. (2005)

Microphysics scheme

Name of scheme	*Nomenclature*	*Selected reference*
Purdue Lin	Lin	Lin et al. (1983)
WRF single-moment 6-class	WSM-6	Hong and Lim (2006)
Thomson scheme	Thomson	Thomson et al. (2004)

2.3 Study III: Evaluation of the WRF PBL parameterizations for both cumulus and stratocumulus

In this study, we aim to investigate the performance of the various WRF PBL schemes in cloud simulations of both marine stratocumulus and shallow cumulus. Meanwhile, we also implement and evaluate the ability of a new scheme (Total-Energy/Mass-Flux) based on the Eddy-Diffusivity/Mass-Flux (EDMF) concepts.

We design a set of several WRF single-column model (SCM) simulations for three well-known large-eddy simulation (LES) case-studies based on field campaigns. Including the TEMF scheme, five PBL parameterizations are examined against LES. Resolving the large eddies which are responsible for the transport of mass, momentum, and energy in the PBL, LES result has been used to serve as a proxy of reality to guide the development of PBL parameterization.

We perform a suite of simulations using the SCM version of WRF for 3 case-studies associated with field experiments, which are chosen because they have been intensively studied using LES models. The three field campaigns are: 1) the second Dynamics and Chemistry of Marine Stratocumulus (DYCOMS-II; Stevens et al., 2003) field study, 2) the Barbados

Oceanographic and Meteorological Experiment (BOMEX; Delnore, 1972), and 3) the Rain in Cumulus over Ocean (RICO; Rauber et al., 2007) experiment (Figure 2). DYCOMS- II took place in the subtropical Pacific, while BOMEX and RICO were in the tropical Atlantic. The marine clouds in BOMEX and RICO are classified as shallow cumulus, while the DYCOMS-II case is classified as stratocumulus.

In addition to TEMF, four other PBL schemes are used: YSU, MYJ, MYNN, and MRF (Hong and Pan, 1996). Note that YSU and MRF are classified as first-order schemes, whereas the others are turbulent kinetic energy closure schemes, in which a prognostic equation is used to determine the eddy diffusivity. In addition, a moist convection parameterization, the Kain-Fritsch scheme, is selected for the non-TEMF SCM simulations of the BOMEX and RICO cases. This allows us to compare the results using the existing WRF PBL schemes with TEMF for shallow cumulus cases. In WRF, the cloud microphysics component estimates the amount of various types of condensed water (i.e., cloud, rain, and ice). Thus, for a given WRF PBL scheme, the estimated cloud liquid water can vary with the choice of microphysics scheme. For each PBL scheme used in this study, we perform nine simulations with each of the nine available microphysics schemes, and the average over the ensembles of simulations using the various microphysics schemes is presented.

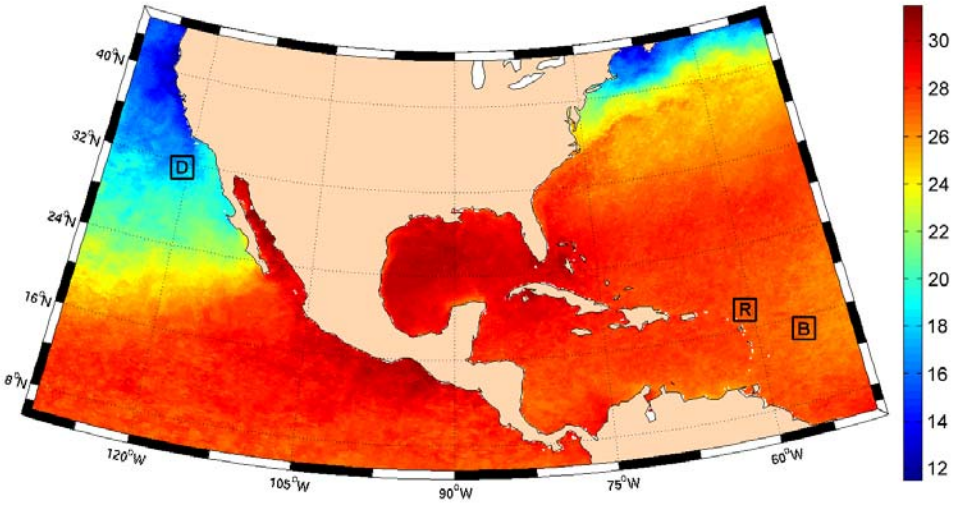

Figure 2: Locations of the selected experiments in this study: the DYCOMS-II (D), the BOMEX (B), and the RICO (R). The color map represents the averaged sea surface temperature of remotely sensed data collected by the AVHRR during July 2001.

3. Results

3.1 Selected results from Study I

3.1.1 Evaluation of WRF simulation

The mean atmospheric circulation in the Southeast Pacific is summarized. Southerly to south-easterly winds prevail between the surface and 700 hPa, veering towards westerlies above that level. The meridian component also changes sign, reflecting the regional imprint of the Hadley circulation. In the upper portion of the marine boundary layer near the coast, a prominent feature is the southerly low-level jet, with a maximum wind core near 950 hPa at 30S.

The WRF simulations broadly capture all of these features. Figure 3 compares the mean zonal and meridional 10-meter winds with QuikSCAT data averaged over the simulated period. In general, there is good agreement both in strength and spatial pattern. The visible difference between simulated and observed zonal wind near the WHOI buoy in the center of the domain (85W, 20S) amounts to an overestimation of about 10%.

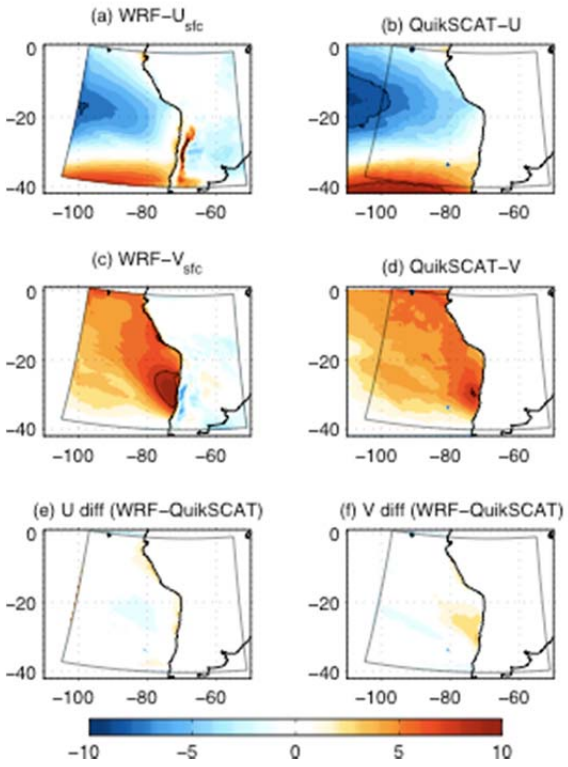

Figure 3: Mean (a) zonal wind for WRF and (b) QuikSCAT, (c) meridian wind for WRF and (d) QuikSCAT, (e) zonal wind difference and (f) meridian wind difference.

In Figure 4, we compare individual temperature and moisture profiles from the simulation with ship-based observations at the locations of the WHOI (20S, 85W) and DART (20S, 75W) buoys made on October 16–19 and October 23, respectively. The simulation reproduces the observed temperature inversion and its zonal tilt, but the boundary layer height is underestimated by about 200–300 m (Figures 4a and 4b). Within the boundary layer, the simulation has a cool bias of about 1–2 K. Figures 4c and 4d show the vertical profiles of specific humidity at both buoy sites, highlighting the reduced cloud-top height compared with observations. Apart from the low height bias, the simulation generally matches the observed moisture structure in the vertical column at the WHOI buoy. At the DART buoy site, however, the simulation also overestimates the moisture content in the mid-troposphere.

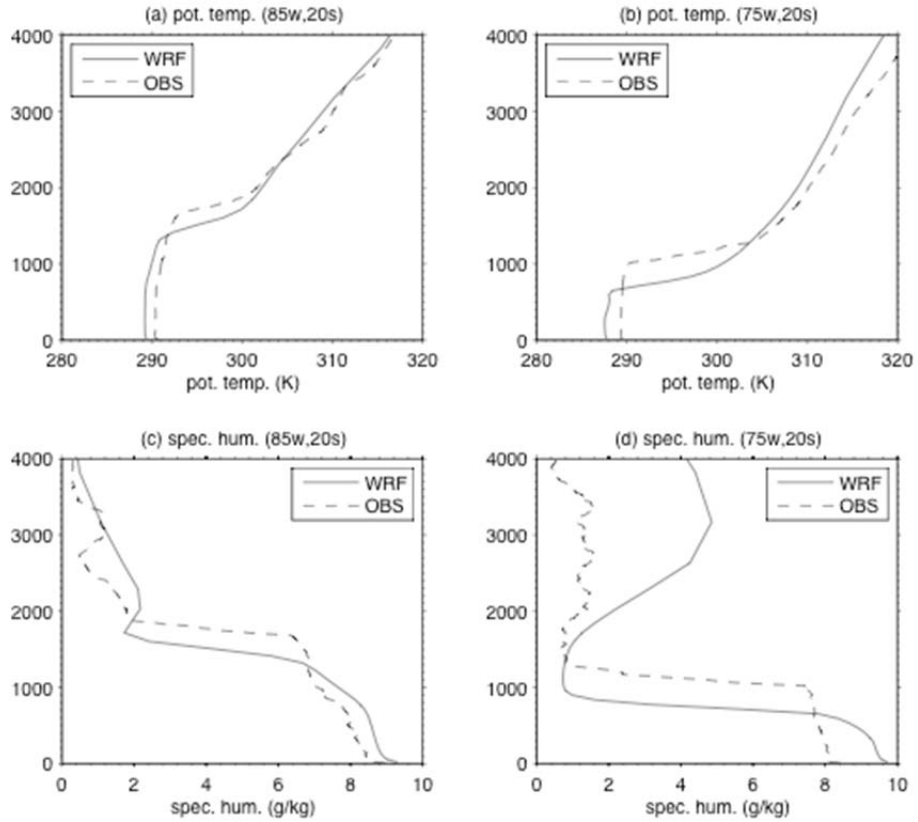

Figure 4: Mean vertical profiles of (a) potential temperature (K), (c) specific humidity (gkg-1) and (e) cloud liquid water (gkg-1) at the WHOI buoy (85W, 20S). (b), (d) and (f) are for the location of the DART buoy (75W, 20S).

3.1.2 Diurnal variability

Figure 5 shows the simulated anomalies, defined as the composite deviations from the daily mean, of the zonal wind on a longitude-height section along 20S and at different times of the mean diurnal cycle. Anomalous onshore westerly appears first at 18:00 UTC just off the coast in the lower troposphere, and peak later at 00:00 UTC with a maximum at 850 hPa. These westerly anomalies gradually vanish, and anomalous offshore easterlies become dominant over the ocean from 9:00 UTC to 15:00 UTC. The maximum diurnal amplitude of the anomalous zonal wind occurs around 700–900 hPa. On the eastern side of the Andes, zonal wind anomalies are nearly out of phase with those over the ocean to the west. This feature is consistent with a strong diurnal cycle of divergence anomalies over the Andes. There is anomalous convergence in the late afternoon, associated with anomalous ascending motion over the Andes, and divergence in the early morning associated with anomalous descending motion.

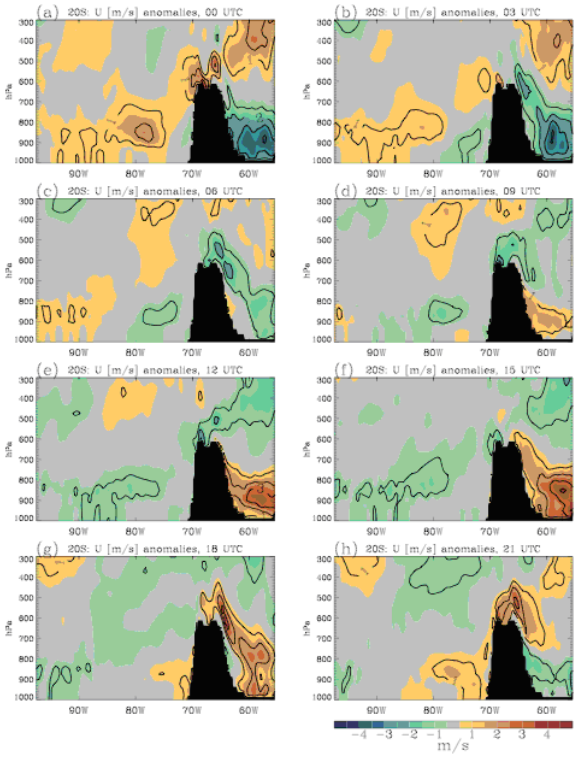

Figure 5: Zonal wind anomalies across 20S latitude at three-hourly intervals for the mean diurnal cycle.

To distinguish the contributions to the variability by diurnal and sub-diurnal components, we perform at each location a harmonic analysis of the vertically integrated horizontal mass flux and its divergence at lower levels. Taken together, the diurnal (24h) and semidiurnal (12h) harmonics of the horizontal mass flux divergence explain more than 70% of the total variance at sub-daily time-scales. The diurnal harmonic generally dominates the diurnal variability of near-surface divergence over open ocean (Figure 6a).

The semidiurnal component is largest along the Peruvian and Chilean coasts (Figure 6b), as well as in areas approaching or poleward of 30S. Figures 6c and 6d depict the phases of the diurnal and semidiurnal harmonics of the horizontal mass divergence. The time of strongest subsidence (positive divergence anomalies) shows distinct propagation patterns. The diurnal harmonic is in phase with the semidiurnal one along the Peruvian coast; the latter component generally lags behind the former moving away from the coast, as expected. Taken together, the features portrayed in Figure 6 suggest the presence of two independent forcings of the divergence anomalies.

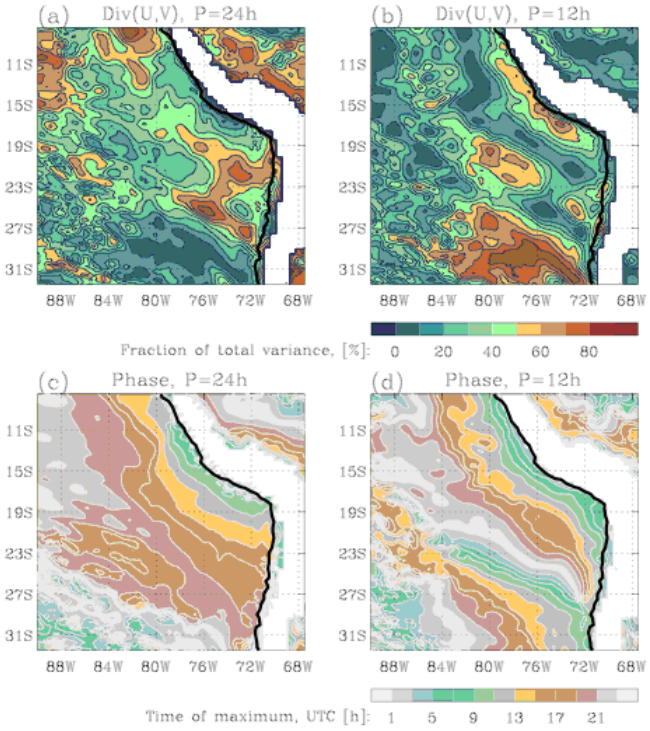

Figure 6: Fractional variance of a) diurnal and b) semidiurnal components of the mean diurnal anomalies of the vertically integrated horizontal mass divergence between 1000 hPa and 800 hPa. Their respective phases are shown in c) and d), indicated as the time of maximum vertical velocity.

3.1.3 Summary

The WRF model's ability to simulate the diurnal mean and mean diurnal variability was validated against *in-situ* observations and reanalysis products. The control integration produces a reasonably realistic simulation of the vertical temperature and humidity structures of the lower troposphere, and of the daily-mean boundary layer circulation and its diurnal variations. Notable biases include an overestimate of the strength of the surface winds and an underestimate of the atmospheric boundary layer height along the Peruvian-Chilean coast.

We decomposed the diurnal variability of the surface circulation into diurnal and semidiurnal harmonics, which together contain most of the total variance. In most oceanic areas, the diurnal component is generally dominant, but bands of strong semidiurnal variations appear parallel to the coastline and near the coast. Above the inversion, vertical wind anomalies with a significant semidiurnal component are common, with increased amplitude near the coast.

The most prominent diurnal signal is associated with ascending motion following daytime heating of the west and south-westward facing slopes of the Andes. The main wave-front travels southwestward, away from southern Peru, over the open ocean. This wave has a primarily diurnal character. Waves of semi-diurnal frequency also emanate from and propagate away from the continent, with a slower speed. Near the coast of Chile this component is the dominant one.

3.2 Selected results from Study II

3.2.1 WRF simulated cloud cover

We show in Figure 7a MODIS low cloud cover (CC) during the months of October and November 2008, averaged over the 4 available phases of the diurnal cycle. This figure highlights the existence of a stratocumulus deck that peaks on average 500 km offshore. This MODIS true CC is very similar to what we defined as the lower bound for MODIS 15-km CC (not shown). Therefore, Figure 7a represents the minimum cloud cover the model must produce to be considered realistic. In Figure 7b, we show the corresponding upper bound for MODIS 15-km CC. It is much more homogeneous than the MODIS true CC, with values greater than 90% over most of the domain. In Figures 7c to 7g, we plot the corresponding results for the WRF 15-km simulations with the five BL schemes tested and with WSM6 as the MP scheme. A stratocumulus deck can be clearly identified in all these experiments. While MYNN (Figure 7h) produces almost as much CC as the upper bound of MODIS 15-km CC, other schemes, such as YSU, slightly underestimate the lower bound for observations. In Figure 7i, we show the experiment using the Tiedtke cumulus scheme. Compared to the corresponding case using the Kain-Fritsch scheme (Figure 7h), the CC maximum is displaced offshore. CC is also significantly reduced overall and well below the lower bound of MODIS 15-km CC.

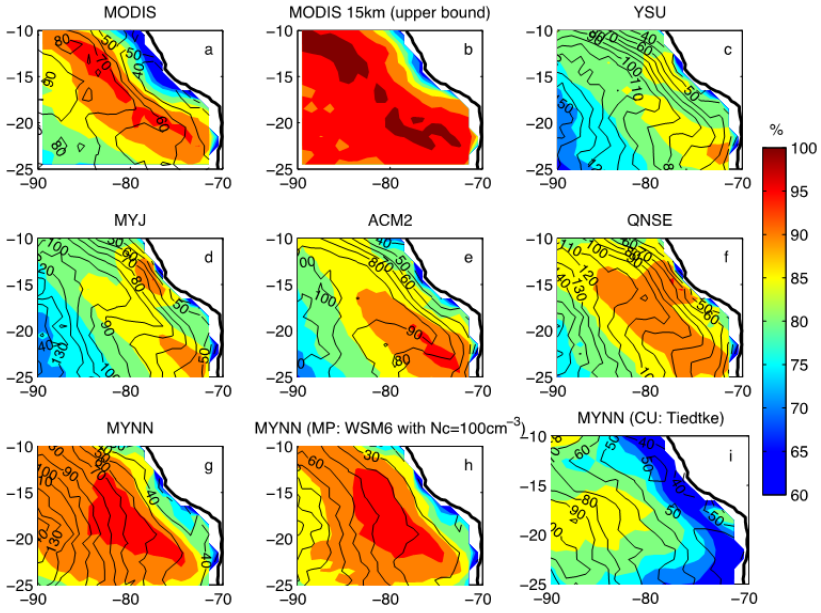

Figure 7: a) MODIS low cloud cover (shaded, %), and MODIS LWP (low cloud events only, contour, g/m2); b) upper bound for MODIS 15-km CC (%, see text for details); WRF 15-km low cloud cover (shaded, %) and LWP (low cloud events only, contour, g/m2) using WSM6 as microphysics scheme and c) YSU, d) MYJ, e) ACM2, f) QNSE, g) MYNN as boundary layer scheme; i) Same as h) but using WSM6 with a droplet concentration of 100 cm-3; j) Same as h) but using the Tiedtke cumulus scheme. Data are averaged between Aqua and Terra overpasses.

3.2.2 WRF simulated cloud properties

In Figure 8, the domain average mean state for liquid water path (LWP), cloud top height (CTH) and cloud depth (CD) are plotted. For LWP (Figure 8a), both MP and BL schemes contribute to the model spread, although MP contributions are greater. Overall, there is an overestimation of MODIS LWP values. The runs using Thomson and Lin as MP are well outside the uncertainty range for observations, with overestimations of 60 to 80% on average. The runs

using WSM6 are closer, with the overestimation reduced to 15% when combined with the BL scheme MYNN. The two experiments using the cumulus schemes, including a shallow cumulus parameterization, show a decrease of the LWP compared to the run using the Kain-Fritsch scheme (with MYNN and WSM6).

For CTH (Figure 8b), the BL schemes are the main contributors to the spread, though contributions from the MP schemes are not negligible. Overall, WRF underestimates CTH. MYNN is generally closest to observations. Values very close to observations are approached when MYNN is combined with Lin or Thomson. However, this agreement may be somewhat misleading, since the clouds produced in these cases significantly overestimate LWP. Figure 8b also highlights the sensitivity to the mixing length for the deepening of the BL in the TKE schemes. In fact, while MYNN and MYJ have similar TKE formulations and differ only in their mixing length expressions, the CTH produced by these two schemes are significantly different, with cloud tops 400 m higher in the MYNN scheme.

WRF generally overestimates CD (Figure 8c), and both BL and MP schemes contribute approximately equally to the spread. As with LWP, Lin and Thomson significantly overestimate CD observations, and WSM6 is closer to truth when combined with MYNN. The two experiments having a shallow cumulus parameterization reduce the CD, and in the case of Tiedtke, the cloud depth is dramatically underestimated, being less than half the observed value.

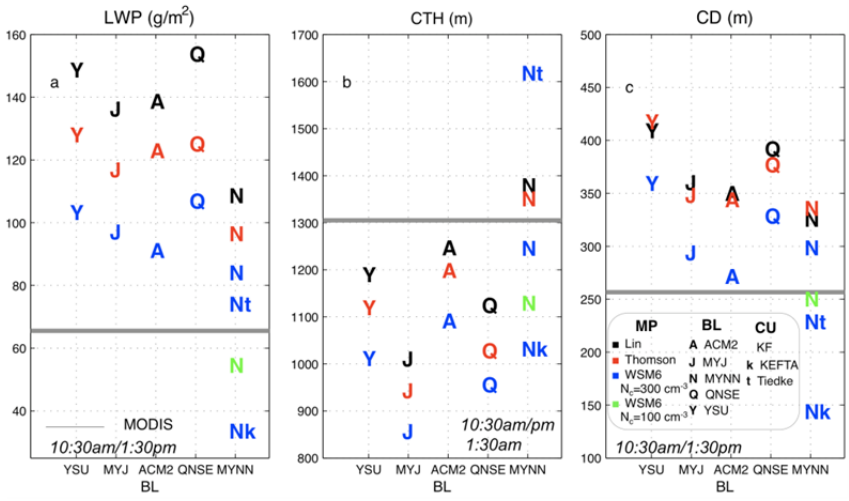

Figure 8: a) WRF 15-km LWP (cloudy scenes only, Ttop>273K, g/m2) averaged over the domain highlighted on Figure 7 in Oct/Nov 2008, and interpolated at MODIS daytime overpass times; b) Same as a), but for cloud top height (CTH<2km), average between MODIS overpasses at 1:30 am and 10:30 am/pm. The gray line represents MODIS CTH; c) Same as a), but for cloud depth. The gray line represents MODIS CD.

3.2.3 Impacts of MP and BL schemes

To quantify more precisely the effect of each scheme, we separate the MP and BL contributions for each cloud variable. The MP (or BL) contribution is relative to the ensemble mean of all MP (or all BL) schemes and is a percentage relative to the mean of our entire set of experiments. The scatter plots in Figure 9 depict the corresponding contributions to variations in CC, LWP, CTH, CD, surface precipitation, and the average relative humidity (RH) in the boundary layer. The more the data points are organized in a vertical line, the more the BL

scheme contributes to the variable in question. The more they are organized horizontally, the greater the contribution of the MP scheme.

The MP contributions are negligible for CC and are relatively small for CTH. For LWP and CD, both MP and BL schemes contribute to the spread, although the MP contribution is slightly more significant in the case of LWP. For precipitation, both MP and BL contribute to the spread. However, the BL spread is mainly due to MYNN. In fact, while other schemes roughly produce 0.7 mm/day of precipitation, the MYNN scheme behaves quite differently than others with average precipitation of 0.2 mm/day, which is closer to the mean value measured during VAMOS Ocean-Cloud-Atmosphere-Land Regional Experiment (~0.1 mm/day; Wood et al., 2010).

Because MP contributions can be directly related to MP parameterizations, we can diagnose mechanisms that control their variability. In particular, we can note that while WSM6 produces more precipitation than other MP schemes, it also produces clouds with less liquid water. This suggests again that auto-conversion controls the MP contribution on LWP. However, the correspondence between the MP contributions to LWP and precipitation is not systematic.

As with the MP contributions, we can interpret BL contributions as being primarily related to BL parameterizations. For example, MYNN simultaneously produces much lower RH, clouds with smaller LWP, and much less precipitation. This suggests that as MYNN produces drier boundary layers, there is overall less water vapor condensation and more liquid water evaporation. As a result, the clouds have smaller LWP and less precipitation is produced.

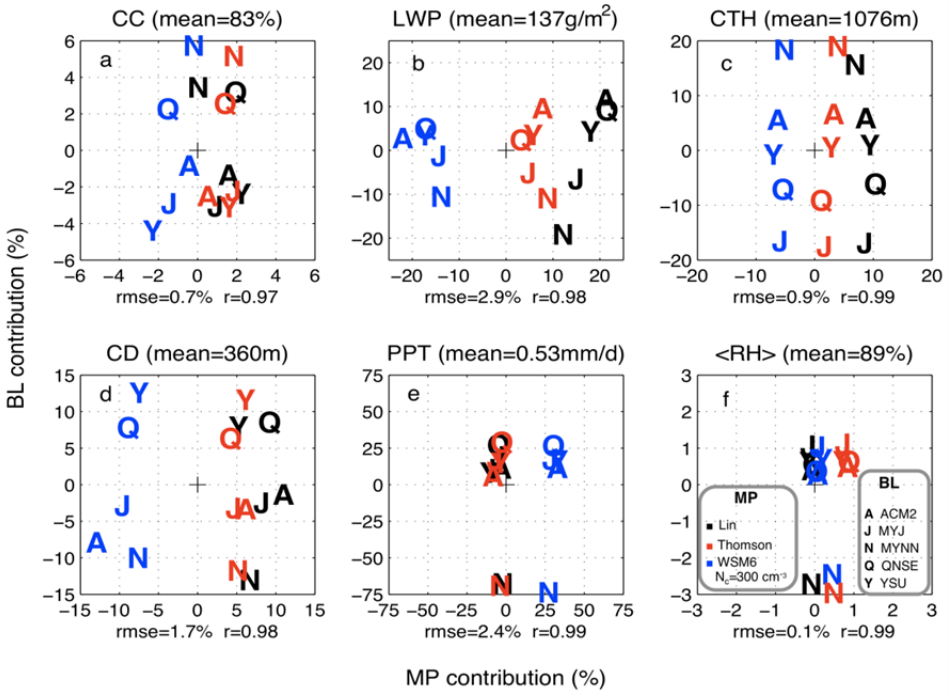

Figure 9: BL contributions versus MP contributions (%) in WRF for a) low cloud cover (CC), b) liquid water path (LWP), c) cloud top height (CTH), d) cloud depth (CD), e) precipitation (PPT), and f) averaged relative humidity in the boundary layer (RH). Each variable is averaged over the domain highlighted in Figure 7 in Oct/Nov 2008 (WRF 3-hourly outputs are averaged).

3.2.4 Summary

Experiments without shallow cumulus parameterization exhibit systematic features. In particular, we demonstrate that feedbacks between MP and BL schemes are minimal in the model. The primary variable that MP schemes contribute to is LWP. The performance for LWP then affects the performance for cloud depth and downward shortwave flux. BL schemes contribute to low clouds in multiple ways. They are the primary contributors to CC and CTH. In this study, we show that model performance for CTH governs the performance for surface energy fluxes and boundary layer structure.

In our study, MYNN is the BL scheme that performs best. With this scheme, the low bias for CC at the diurnal minimum is less than 10%, and the one for CTH is less than 100 m. As a result of these greater CTHs, the high bias for average relative humidity is reduced to 5% (10% with other BL schemes). By reducing RH, MYNN has also the ability to reduce LWP and precipitation, bringing them closer to observations. Thus, the overall better behavior of MYNN can be attributed to a better representation of the BL height.

This suggests that an appropriate tuning of CTH would likely improve the representation of low cloud in the model. However, such tuning is not an easy task as the balance between various turbulent processes is very sensitive. Current TKE schemes fail in finding a good compromise between turbulent mixing processes that deepen the BL and small scale mixing that contributes to entrainment. For example, in the case of MYNN, BL deepening is promoted in comparison to other schemes, but the average degree of adiabaticity is greater than observed, suggesting that entrainment processes are too weak.

A missing piece in all the schemes might be the turbulent radiative cooling at the cloud top. In fact, this process is recognized as a major physical contribution to BL deepening and mixing. However, it is only represented implicitly in TKE schemes such as MYNN and therefore, it is likely underestimated. We suspect some compatibility issues with the current version of WRF, and expect improvements in future versions.

3.3 Selected results from Study III

3.3.1 EDMF and TEMF PBL parameterizations

Rather than a specific parameterization, Eddy-Diffusivity/Mass-Flux (EDMF; Siebesma and Teixeira, 2000) is an approach based on an optimal combination of the eddy-diffusivity (ED) parameterization, used to simulate turbulence within the PBL, and the mass-flux (MF) parameterization, used for moist convection. Though differences in the details are present in different EDMF implementations on weather or climate models, the fundamental idea is the same: Local mixing is parameterized by the ED term, while the non-local transport due to convective thermals is represented by the MF term. The main difference between Total-Energy/Mass-Flux (TEMF; Angevine et al., 2010) and EDMF is in the calculation of the ED coefficient: EDMF often uses turbulent kinetic energy, whereas TEMF uses total turbulent energy for better handling of stably-stratified conditions (Mauritsen et al., 2007). This advanced TEMF scheme is implemented in WRF version 3.1 and evaluated in this work.

3.3.2 Performance on stratocumulus case (DYCOMS-II)

While all liquid-water potential temperature profiles are within the range of the LES ensemble, there are slight differences in the inversion of the PBL (Figure 10a). In particular, near the entrainment zone the MRF parameterization creates a small temperature inversion, which could be an issue due to numerical instability. All SCM experiments simulate comparable profiles of total water mixing ratio, but a small overestimate within the PBL is seen (Figure 10b).

No significant difference is seen across PBL schemes (Figure 10c) mostly because this plot uses a log-scale and the cloud cover in this stratocumulus case is close to 1. Estimates of cloud in the MYNN and TEMF experiments are quite close to LES, while larger values are simulated by YSU and MRF and smaller value is performed by MYJ.

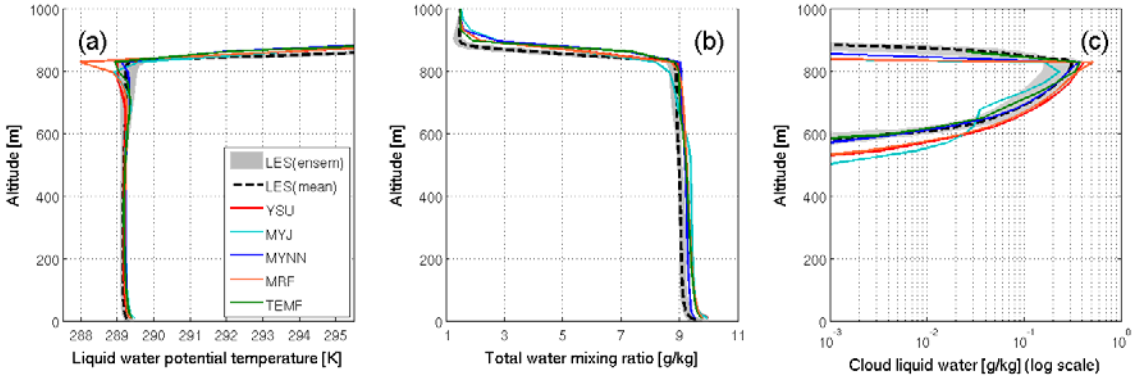

Figure 10: Vertical profile of a) liquid water potential temperature, b) total water vapor mixing ratio, and c) cloud liquid water (in log-scale) for the DYCOMS-II experiments.

3.3.3 Performance on shallow cumulus case (BOMEX and RICO)

Figure 11 shows the vertical profiles from the BOMEX case. For potential temperature, TEMF and MYNN provide the most realistic profiles, while MYJ is too cold and shallow, and YSU leads to sub-cloud layers that are too deep (Figure 11a). For water vapor mixing ratio (Figure 11b), the parameterizations show similar biases. The significant differences between the parameterizations are clear for cloud liquid water. The cloud profiles from all PBL parameterizations are significantly larger than LES (Figure 11c). Essentially, this shows the dangers of the unphysical coupling between boundary layer, convection, and cloud microphysics parameterizations in the WRF model. In addition, the SCM liquid water vertical structures shown in Figure 11c are profoundly different from one another. The liquid water profiles that better resemble the LES results are seen in TEMF (and to a certain extent MYNN) with realistic cloud base and cloud top heights. YSU and MRF produce clouds that are too shallow with very large peak values, while MYJ produces a very shallow cloud.

The RICO results (not shown) overall are similar to BOMEX, which shows the robustness (or lack of it) of the various schemes. The TEMF (and to a certain extent MYNN) parameterization is again superior to the others, producing cloud profiles that are relatively close to the LES ensembles.

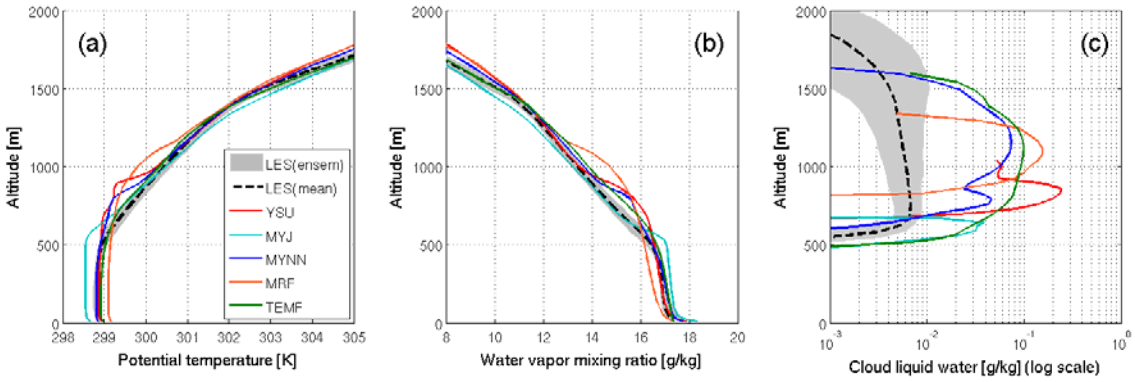

Figure 11: Vertical profile of a) potential temperature, b) water vapor mixing ratio, and c) cloud liquid water (in log-scale) for the BOMEX experiments.

3.3.4 Summary

For the stratocumulus case, all models produce a similar structure of cloud liquid water but with some differences in terms of absolute values. For both shallow cumulus cases, the results are fairly similar with TEMF, and to a certain extent MYNN, producing superior depictions of the thermodynamical vertical structure. All SCMs clearly overestimate the values of liquid water when compared to the LES results, mostly because of the unphysical coupling between boundary layer and cloud microphysics parameterizations in WRF. In spite of this large positive bias, the TEMF version produces realistic cloud base and cloud heights for both BOMEX and RICO.

A parameterization based on the EDMF approach (i.e., TEMF) that unifies different components produces a better result when compared with LES, with realistic vertical structures for stratocumulus and cumulus regimes. Existing PBL parameterizations in WRF are not able to produce fully realistic results when simulating stratocumulus and shallow cumulus regimes. The often artificial modularity of parameterizations as they are implemented in WRF produces unreliable results that are virtually impossible to interpret due to the plethora of available parameterizations and their coupling.

4. Publications/presentations from this project

4.1 Journal publications

Toniazzo, T., F. Sun, C. R. Mechoso, and A. Hall, 2013: A regional modeling study of the diurnal cycle in the lower troposphere in the south-eastern tropical Pacific, *Climate Dynamics*, published online.

Huang, H.-Y., A. Hall, and J. Teixeira, 2013: Evaluation of the WRF PBL parameterizations for marine boundary layer clouds: Cumulus and stratocumulus, *Monthly Weather Review*, 141, 7, 2265–2271.

Jousse, A., A. Hall, F. Sun, and J. Teixeira: How do parameterizations affect the stratocumulus structure in WRF?, In preparation to submit to Journal of Atmospheric Sciences.

4.2 Presentations

Huang, H.-Y., A. Hall, and J. Teixeira, 2010: Evaluation of the total energy mass flux boundary layer scheme in the WRF model using DYCOMS2 data, Eos Trans., American Geophysical Union, Fall Annual Meeting.

Sun, F., T. Toniazzo, C. R. Mechoso, and A. Hall, 2010: Regional modeling studies on the diurnal and semidiurnal cycles of boundary layer off the west coast of South America, Eos Trans., American Geophysical Union, Fall Annual Meeting.

Huang, H.-Y., A. Hall, and J. Teixeira, 2011: Evaluation of the total energy-mass flux boundary layer scheme in the WRF model for marine boundary layer cloud regions, Department of Energy, Climate Modeling Principal Investigator Meeting.

Jousse, A., A. Hall, F. Sun, and J. Teixeira, 2012: Stratocumulus simulations over the southeast Pacific: an evaluation of the parameterizations in WRF, Eos Trans., American Geophysical Union, Fall Annual Meeting.

5. References

Angevine, W. M., H. Jiang, and T. Mauritsen, 2010: Performance of an eddy diffusivity-mass flux scheme for shallow cumulus boundary layers. *Mon. Wea. Rev.*, 138, 2895-2912.

Dee, P., and Co-authors, 2011: The ERA-Interim reanalysis: configuration and performance of the data assimilation system. *Quart. J. Roy. Meteor.*, 137, 553-597.

Delnore, V. E., 1972: Diurnal variation of temperature and energy budget for the oceanic mixed layer during BOMEX. *J. Phys. Oceanogr.*, 2, 239-247.

Hong, S.-Y., and J.-O. J. Lim, 2006: The WRF single-moment 6-class microphysics scheme (WSM6). *J. Korean Meteor. Soc.*, 42, 129-151.

Hong, S.-Y., and H.-L. Pan, 1996: Nonlocal boundary layer vertical diffusion in a medium-range forecast model. *Mon. Wea. Rev.*, 124, 2322-2339.

Janjic, Z. I., 2002: Nonsingular Implementation of the Mellor-Yamada Level 2.5 Scheme in the NCEP Meso model. *NCEP Office Note*, 437, 61 pp.

Kain, J. S., and J. M. Fritsch, 1993: Convective parameterization for mesoscale models: The Kain-Fritcsh scheme. *The representation of cumulus convection in numerical models*, K. A. Emanuel and D.J. Raymond, Eds., Amer. Meteor. Soc., 246 pp.

Klein, S. A., and D. L. Hartmann, 1993: The seasonal cycle of low stratiform clouds. *J. Climate*, 6, 1587-1606.

Lin, Y.-L., R. D. Farley, and H. D. Orville, 1983: Bulk parameterization of the snow field in a cloud model. *J. Climate Appl. Meteor.*, 22, 1065-1092.

Nakanishi, M. and H. Niino, 2004: An improved Mellor-Yamada level-3 model with condensation physics: Its design and verification. *Bound.-Layer Meteor.*, 112, 1-31.

Mauritsen, T., G. Svensson, S. S. Zilitinkevich, I. Esau, L. Enger, and B. Grisogono, 2007: A total turbulent energy closure model for neutrally and stably stratified atmospheric boundary layers. *J. Atmos. Sci.*, 64, 4113-4126.

Mellor, G. L., and T. Yamada, 1982: Development of a turbulence closure model for geophysical fluid problems. *Rev. Geophys. Space Phys.*, 20, 851-875.

Platnick, S., and Co-authors, 2003: The MODIS cloud products: Algorithms and examples from Terra, IEEE Trans. *Geosci. Remote Sens.*, 41, 459-473.

Platnick, S., and M. D. King, 2007: Update on the MODIS Collection 5 Processing Cloud Optical and Microphysical Algorithm and Product Validation, in Fourier Transform

Spectroscopy/Hyperspectral Imaging and Sounding of the Environment, OSA Tech. Digest Ser. Pap. HTuA1 [CD-ROM], Opt. Soc. of Am., Washington, D. C.

Pleim, J. E., 2007: A combined local and nonlocal closure model for the atmospheric boundary layer. Part I: Model description and testing. *J. Appl. Meteor. Climatol.*, 46, 1383-1395.

Rauber, R. M., and Co-authors, 2007: Rain in shallow cumulus over the ocean – The RICO campaign. *Bull. Am. Meteorol. Soc.*, 88, 1912-1928.

Reynolds, R. W. and T. M. Smith, 1994: Improved global sea surface temperature analyses. *J. Climate*, 7, 929-948.

Siebesma, A. P., and J. Teixeira, 2000: An advection-diffusion scheme for the convective boundary layer: Description and 1D results. *14th Symposium on Boundary Layers and Turbulence*, Aspen, CO, Amer. Meteor. Soc., 133-136.

Stevens, B., and Co-authors, 2003: Dynamics and chemistry of marine stratocumulus - DYCOMS-II. *Bull. Amer. Meteor. Soc.*, 84, 579-593.

Stevens, B., and Co-authors, 2007: On the structure of the lower troposphere in the summertime stratocumulus regimes of the Northeast Pacific. *Mon. Wea. Rev.*, 135, 985-1005.

Sukoriansky, S., B. Galperin, and V. Perov, 2005: Application of a new spectral theory of stable stratified turbulence to the atmospheric boundary layer over sea ice. *Bound. Layer Meteorol.*, 117, 231-257.

Teixeira, J., and Co-authors, 2011: Tropical and sub-tropical cloud transitions in weather and climate prediction models: the GCSS/WGNE Pacific Cross-section Intercomparison (GPCI). *J. Clim.*, 24, 5223-5256.

Thompson, G., R. M. Rasmussen, and K. Manning, 2004: Explicit forecasts of winter precipitation using an improved bulk microphysics scheme. Part I: Description and sensitivity analysis, *Mon. Wea. Rev.*, 132, 519-542.

Wood, R., and Co-authors, 2010: The VAMOS Ocean-Cloud-Atmosphere-Land Study Regional Experiment (VOCALS-REx): goals, platforms, and field operations, *Atmos. Chem. Phys. Discuss.*, 10, 20769-20822.